

Effects of SiO₂-based scaffolds in TiO₂ photocatalyzed CO₂ reduction

Danny Zanardo ^a, Giulia Forghieri ^a, Sebastiano Tieuli ^a, Elena Ghedini ^a, Federica Menegazzo ^a, Alessandro Di Michele ^b, Giuseppe Cruciani ^c, Michela Signoretto ^{a,*}

^aCATMAT Lab, Department of Molecular Sciences and Nanosystems, Ca' Foscari University Venice and INSTM-RU center and consortium, Via Torino 155, 30172 Venezia Mestre, Italy

^bDepartment of Physics and Geology, University of Perugia, Via Pascoli, 06123 Perugia, Italy

^cDepartment of Physics and Earth Science, University of Ferrara, Via Saragat 1, 44122 Ferrara, Italy

* Corresponding author. Email address: miky@unive.it

Abstract

CO₂ photoreduction has claimed as appealing process to upgrade a waste gas into valuable fuels or chemicals. Titanium dioxide (TiO₂) is one of the most popular material used as catalyst for this reaction, having however a poor activity. The utilization of transparent, insulating and highly porous scaffolds to support a photoactive phase has been reported as one of the possible strategies to improve the performances of this material. In this work, two silica-based materials with different porosity type and level, were involved as support for the TiO₂ and assessed in the gas-phase CO₂ photoreduction with H₂O. The morphological, structural and surface properties were then evaluated by means of different characterization techniques, aiming to correlate them with the catalytic activity and selectivity. The TiO₂-SiO₂ composites revealed a comparable activity compared to pure TiO₂, despite the low fraction of photoactive phase due to improved light harvesting and reagents adsorption on the composites. The CO₂ capture/photoconverting ability was evaluated, to explore the potentiality as multifunctional material.

Keywords

Carbon dioxide; photoreduction; titanium dioxide; silica; scaffolding.

1. Introduction

CO₂ chemical conversion has been addressed as appealing technologies to upgrade a low-value and abundant raw material (CO₂) into valuable carbon-based fuels or chemicals [1]. Among the proposed processes, photocatalysis is an interesting choice due to the utilization of very mild reaction conditions and the potential exploitation of sunlight as energy source [2-4]. Several semiconductor (SC) materials have been studied for this reaction, and titanium dioxide (TiO₂) is the most popular being abundant, cheap, photostable and non-toxic [5]. However, many issues negatively affect this photocatalyst: (i) wide bandgap (3-3.3 eV) which allows the exploitation of UV photons only (ca. 5% of the incoming sunlight); (ii) fast charge carrier recombination and (iii) slow kinetics in some charge carrier surface transfer processes, i.e. CO₂ or proton reduction [6]. To overcome these limitations, several material modifications have been proposed, such visible-light sensitization with narrow bandgap SCs [7,8] or the surface functionalization with co-catalysts to improve the reaction kinetics [9,10]. Another appealing material design strategy is the utilization of an insulating, transparent and porous material such as silica (SiO₂), as scaffold supporting the photoactive phase, to

improve the reagents adsorption [11,12]. The direct incorporation of Ti^{4+} cations within silica matrix has been observed to provide tetrahedral Ti^{4+} species, affording a blue-shift in the absorption edge and an improved photocatalytic activity compared to bulk TiO_2 [12,13]. Despite the effectiveness of such tetrahedral species, the absorption edge blue-shift is detrimental for a wide band-gap material like TiO_2 , because it requires more energetic and harmful UV radiation to make it active. TiO_2 -based nanoparticles (NPs), exhibiting the typical absorption band edge at ca. 3.3 eV, have been successfully loaded onto mesoporous silica materials such as SBA-15 [11,14] or COK-12 [15], leading to an activity improvement compared to the bare TiO_2 NPs. Besides the improved reagents adsorption, the improved photon harvesting through light scattering was also proposed as a potential effect in improving the activity [11]. In this regard, Wang *et al.* observed an increased activity toward CO_2 photoreduction on a $g-C_3N_4$ photocatalyst treated with a transparent layer of reconstructed cellulose, that boosts up the light absorption and consequent photon utilization, by means of the light scattering phenomenon [16]. Besides the activity improvement, the scaffold was observed to play an important role in determining the selectivity of the photoreduction process as well. Indeed, the presence of a mesoporous scaffold was observed to enhance the formation of highly reduced carbon products (CH_4 vs CO) on Ce-promoted TiO_2 [17], while the moiety (hydroxyl groups) on the scaffold surface was observed to play an important role in determining the CH_4 vs CH_3OH selectivity on a Ti-modified β -zeolite photocatalyst [12]. Tasbihi *et al.* observed also an improved yield of hydrogen (H_2) by supporting TiO_2 onto a mesoporous silica [15]. H_2 is generally considered as a side product in CO_2 photoreduction, since it consumes both photogenerated electrons and the reductant (H_2O) to generate an unwanted product (H_2) [18]. Thus, several strategies have been adopted to inhibit this side reaction, either by using a CO_2 -rich reaction medium [19] or by surface modification with alkaline materials (i.e. MgO) [18]. The former, despite being widely exploited in CO_2 photoconversion, could represent a bottleneck in future large-scale application, because largely available as a diluted source (i.e. flue gases) [20] and an intermediate enrichment step would be required [21]. Liu *et al.* reported a TiO_2 photocatalyst supported onto a mesoporous alkaline scaffold, able to adsorb CO_2 in the dark, thanks to the alkaline support, and then reducing it upon irradiation in quite harsh conditions ($T > 100^\circ C$), thus acting as a hybrid capture-photoconverting system [22]. To the best of authors' knowledge, this is the only reported work concerning a multifunctional system for CO_2 capture and photoconversion.

So far, most attention has been paid to the use of high-surface area mesoporous transparent materials due to their effectiveness as scaffolds in improving the CO_2 photoconversion efficiency. However, to the best of our knowledge, no macroporous materials have been tested yet and, in particular, a comparison between the effect of a macro- and mesoporous scaffold on the photocatalytic performances of TiO_2 has not been reported yet.

Through this work, a benchmark TiO_2 material was supported on two different SiO_2 -based scaffolds: a crystalline silica support with macroporosity and a material with an ordered distribution of mesopores defined by amorphous walls (SBA-15). Gas-phase CO_2 photoreduction activity and selectivity of the synthesized

materials were then compared and correlated to their physical-chemical properties. Finally, such materials were assessed as hybrid CO₂ capture-photoconverting systems in mild conditions.

2. Experimental part

2.1. Materials

The following materials were used as-received: benchmark TiO₂ (P25, Evonik), SiO₂ (quartz, size > 230 mesh, Sigma Aldrich), tetraethylortosilicate (TEOS, assay 98%, Sigma Aldrich), triblock copolymer (Pluronic P123, EO₂₀-PO₇₀-EO₂₀, Sigma Aldrich), isopropanol (assay 99.8%, Sigma Aldrich) and aqueous HCl (assay 37%, Sigma Aldrich).

2.2. Catalyst preparation.

2.2.1. SBA-15 synthesis.

SBA-15 was prepared according to a previous reported method [23]. The template (P123) was dissolved in aqueous HCl and TEOS was then slowly added as silica precursor. The mixture was stirred at r.t. for 24 h and then aged in a sealed Teflon vessel at 95°C for 42 h. The obtained solid was then washed with deionized water, filtered, dried at 110°C for 18 h and finally annealed at 550°C for 6 h in air flow (50 mL/min).

2.2.2. TiO₂-SiO₂ composites synthesis.

The TiO₂-SiO₂ composites were prepared by incipient wetness impregnation [24]. An appropriate amount of P25 (benchmark TiO₂) was dispersed in isopropanol and sonicated for 1 h. The mixture was then impregnated on both benchmark SiO₂ and synthesized SBA-15, loading a 10 wt. % TiO₂. The composites were finally air-dried at 110°C for 18 h. The samples were labelled as follow:

- TiO₂, pristine P25
- ST10, benchmark SiO₂ with 10 wt. % of P25
- SBT10, SBA-15 with 10 wt. % of P25

2.2.3. Characterizations

X-ray diffraction (XRD) patterns were collected on a Bruker D8 Advance DaVinci powder diffractometer using a sealed X-ray tube (copper anode; operating conditions, 40 kV and 40 mA) and a linear array detector (LynxEye), set to discriminate the Cu K α radiation, coupled with a Ni filter to completely remove the Cu K β component. The samples were spun during data collection and a vertical knife was used to avoid low angle air scattering contribution. Data scans were performed in the 2 θ range 5–90° with 0.02° step size and point-detector equivalent counting times of 5 s/step. Quantitative phase analysis and crystallite size determination were performed using the Rietveld method as implemented in the TOPAS v.5 program (Bruker AXS) using the fundamental parameters approach for line-profile fitting. The determination of the crystallite size was

accomplished by the Double-Voigt approach and calculated as volume-weighted mean column heights based on integral breadths of peaks. N₂ physisorption analyses were performed using a Micromeritics TriStar II Plus analyser, recording the adsorption–desorption isotherms at – 196 °C. All samples were previously outgassed at 200°C for 2 h. The surface area was evaluated using the standard BET equation [25]. The morphology and composition were examined by Field Emission Electron Scanning Microscopy (FE-SEM) LEO 1525 ZEISS. Elemental composition and chemical mapping were determined using a Bruker Quantax EDS. The samples were deposited on adhesive carbon tape and metallized with chromium. The morphology was also evaluated by a Transmission Electron Microscopy (TEM) JEOL 3010-UHR instrument operating at 300 kV and equipped with a LaB₆ filament. Digital micrographs were acquired by a Gatan (2k × 2k)-pixel Ultrascan1000 CCD camera. The sample were dry dispersed onto Cu grids coated with lacey carbon before analysis. The FTIR spectra were collected through a Perkin Elmer Spectrum one spectrophotometer in the 4000–400 cm⁻¹ range, dispersing the powders in a KBr pellet. The UV-vis spectra were measured by diffuse reflectance spectroscopy (DRS) by a Cary100 UV-vis spectrophotometer equipped with an integrating sphere, using a BaSO₄ as internal reference, in the 200–800 nm range and 600 nm·s⁻¹ scan rate. The spectra were plotted through the Kubelka-Munk function [26], where R_{∞} is the reflectance of an infinite thick layer:

$$f(R_{\infty}) = \frac{(1 - R_{\infty})^2}{2R_{\infty}}$$

The bandgap (E_g) value was determined through the Tauc relation [27], plotting $(f(R_{\infty})hv)^{1/2}$ vs E (eV). The temperature programmed desorption (TPD) analyses were carried out in a lab-made equipment. The sample was placed in quartz reactor firstly outgassed at 300°C in He flow (40 mL·min⁻¹), then heated from r.t. to 500°C (heating rate 10 °C·min⁻¹), analysing the gas composition through a Gow-mac TCD detector. The CO₂-TPD analysis were carried out through the same procedure but exposing the outgassed sample to a flow of pure CO₂ prior to the TPD analysis.

2.2.4. Photocatalytic tests.

The CO₂ photoconversion reactivity tests were carried out in gas-phase using a flat-type glass photoreactor [10]. The photocatalyst was immobilized onto the irradiated side of the reactor by suspending it in isopropanol and evaporating the solvent within the photoreactor. A CO₂/H₂O mixture (13.3 molar ratio) was produced by bubbling CO₂ (99.9%) through a milli Q water-filled bubbler kept at 40 °C. A medium-pressure Hg lamp (125 W, Helios Italquartz) with a 365 nm main emission line was used as light source, with a 60 W·m⁻² light intensity, controlled with a Delta Ohm HD 2302.0 photo-radiometer and a LP 471 probe. The reaction was carried out, after getting a stable CO₂/H₂O mixture, in static conditions for 6 h, at 70°C (heat from the lamp) and atmospheric pressure. The reaction mixtures were analysed through a 6890 HP gas chromatographer, equipped with a Porapak Q packed column, a TCD detector and an automatic sampling valve. Each reaction was repeated twice. The CO₂ capture-photoconverting tests were performed by running

the reaction in the same conditions above reported but using a CO₂-free He/H₂O mixture (13.3 molar ratio) as reaction medium. The used catalyst was then left on a 10 mol. % CO₂/He stream for 18 h in dark, before re-using it for the reaction with the He/H₂O mixture under irradiation. This procedure was repeated twice.

The turnover frequency (TOF) for CH₄, H₂ or O₂ was calculated as follow:

$$TOF = \frac{mol_P}{m_{CAT} \cdot \tau}$$

where mol_P are the produced moles of CH₄, H₂ or O₂, m_{CAT} the photocatalyst mass and τ the reaction time.

The reaction selectivity (S_P) to a given reduction product (P), was calculated as follow:

$$S_P = \frac{mol_P}{mol_{H_2} + mol_{CH_4}}$$

where mol_{H_2} and mol_{CH_4} are the produced moles of CH₄ and H₂, respectively.

3. Results and discussion.

3.2. Photocatalysts characterizations

The bare TiO₂ is a crystalline material composed of a mixture of anatase (89%) and rutile (11%), as evidenced by XRD reported in Figure S1a, with an averaged crystallite size of 18 nm. The physisorption analysis (Figure S1b) highlights the macro-mesoporous nature of such material due to the hysteresis close to P/P⁰ = 1, with an average specific surface area (SSA) of 50 m²·g⁻¹. Regarding the morphology, it is well known that this kind of material is composed of roughly spherical NPs of ca. 20-40 nm in size [28]. The optical properties, analysed through UV-vis DRS, revealed an absorption band edge below 400 nm (Figure S2a), completely lying in the UV region, and an assessed bandgap (E_g) value of 3.05 eV (Figure S2b), in agreement with literature reports [29].

The SiO₂-TiO₂ composites were prepared by loading 10 wt. % of TiO₂ on the two silica-based support, SiO₂ and SBA-15, aiming to compare the effect of these scaffolds on TiO₂ physical-chemical properties and photocatalytic performances. The SiO₂-TiO₂ composites revealed a notable difference in term of SSA. The bare SBA-15 exhibited a typical type IV isotherm of a mesoporous material, and the presence of uniform cylindrical shaped pores by the sharp hysteresis loop (Figure 1a, dashed line). The morphology of pores can be observed more in details by TEM analyses, where uniform and well-aligned cylindrical pores were found (Figure S3b and S3c). Upon loading TiO₂ on SBA-15, the physisorption hysteresis changes (Figure 1a, straight line) and the SSA slightly decreases from 866 m²·g⁻¹ to 802 m²·g⁻¹, suggesting a comparable porosity of the two materials. On the contrary, the pristine SiO₂ showed a type III hysteresis (Figure 1b, dashed line), related to macroporous materials with very low SSA, which cannot be quantified by the BET model. Upon loading

ha formattato: Tipo di carattere: 11 pt

ha formattato: Tipo di carattere: 11 pt, Non Corsivo, Controllo ortografia e grammatica

ha formattato: Tipo di carattere: 11 pt

ha formattato: Tipo di carattere: 11 pt, Non Corsivo, Controllo ortografia e grammatica

ha formattato: Tipo di carattere: 11 pt

ha formattato: Tipo di carattere: 11 pt, Non Corsivo, Controllo ortografia e grammatica

TiO₂, a sharp hysteresis close to P/P⁰ = 1 appeared (Figure 1b, straight line), pointing out the appearance of some mesopores, ascribable to the loading of TiO₂ NPs.

ha formattato: Tipo di carattere: 11 pt
 ha formattato: Tipo di carattere: 11 pt, Non Corsivo, Controllo ortografia e grammatica

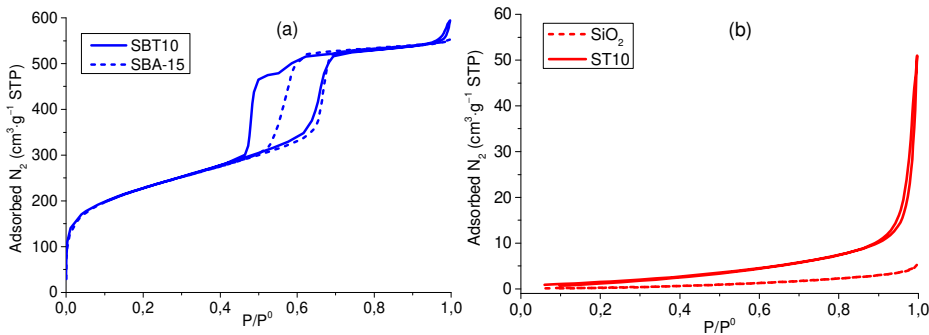


Figure 1. (a) Physisorption isotherms of SBA-15 (dashed line) vs SBT10 (straight line); (b) physisorption isotherms of SiO₂ (dashed line) vs ST10 (straight line).

The diffraction pattern of the two scaffolds revealed some more differences. SBA-15 is an amorphous silica material exhibiting a nanometer-sized ordered pores structure [23]. SiO₂, on the contrary, was found to be a crystalline material composed mainly of quartz (SiO₂, 90.4%) with a small amount of feldspar microcline (KAlSi₃O₈, 9.6%) as impurity (Figure 2). On SiO₂-TiO₂ composites, due to the mild thermal treatment (110°C), the TiO₂ phase composition and crystallite size were supposed to be comparable with the pristine material, as high-temperature thermal treatment are usually required to modify these properties [30].

ha formattato: Tipo di carattere: 11 pt
 ha formattato: Tipo di carattere: 11 pt, Non Corsivo, Controllo ortografia e grammatica

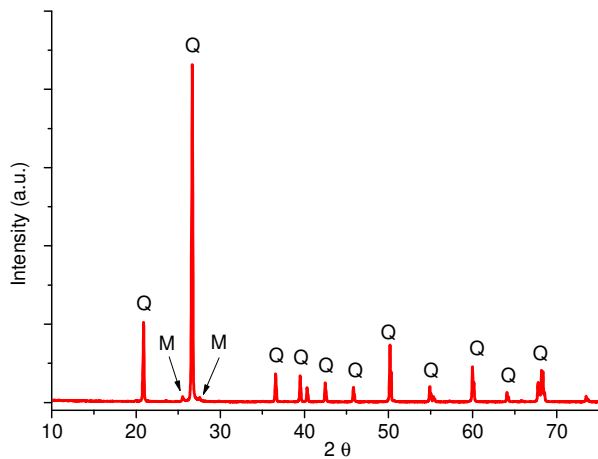


Figure 2. XRD diffractogram of pure SiO₂ scaffold. Crystal phases: quartz (Q), microcline (M).

The morphology was examined through scanning electron microscopy (SEM). ST10 is composed of big micrometer-sized quartz particles (Figure 3a), decorated on the surface by the TiO₂ NPs (Figure 3c), as observable by Ti elemental mapping too (Figure 3e). The TiO₂ surface decoration can be further confirmed comparing the pristine SiO₂ that, contrary to rough ST10, revealed a relatively smooth surface (Figure S4). K and Al were found through the EDX analysis (Figure 3f), supporting the presence of potassium aluminosilicate (microcline) observed by XRD analysis.

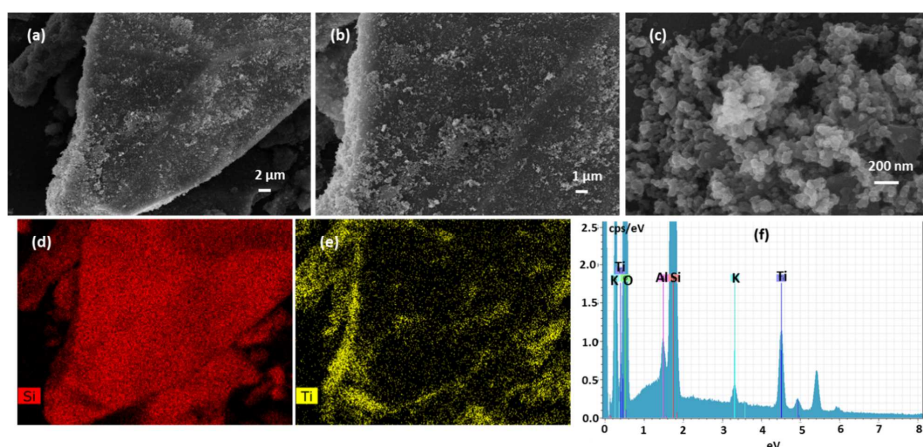


Figure 3. (a), (b), (c) SEM images of ST10; (d) Si elemental mapping; (e) Ti elemental mapping; (f) EDX spectrum.

On the SBT10, micrometre-sized bean-shaped particles of the scaffold, can be recognized (Figure 4a and 6b). As for ST10, the SBA-15 surface is observed to be decorated by agglomerates of TiO₂ NPs (Figure 4b and 6c), also confirmed by the elemental mapping (Figure 4e).

On both the SiO₂-TiO₂ composite (ST10 and SBT10), the TiO₂ NPs morphology was supposed to be comparable with the pure TiO₂ as high-temperature ($T > 400^{\circ}\text{C}$) [30] or hydrothermal [31] treatments, known to induce morphological alternation on the material, were not involved to prepare the composites.

ha formattato: Tipo di carattere: 11 pt

ha formattato: Tipo di carattere: 11 pt, Non Corsivo, Controllo ortografia e grammatica

ha formattato: Tipo di carattere: 11 pt

ha formattato: Tipo di carattere: 11 pt, Non Corsivo, Controllo ortografia e grammatica

ha formattato: Tipo di carattere: 11 pt

ha formattato: Tipo di carattere: 11 pt, Non Corsivo, Controllo ortografia e grammatica

ha formattato: Tipo di carattere: 11 pt

ha formattato: Tipo di carattere: 11 pt, Non Corsivo, Controllo ortografia e grammatica

ha formattato: Tipo di carattere: 11 pt

ha formattato: Tipo di carattere: 11 pt, Non Corsivo, Controllo ortografia e grammatica

ha formattato: Tipo di carattere: 11 pt

ha formattato: Tipo di carattere: 11 pt, Non Corsivo, Controllo ortografia e grammatica

ha formattato: Tipo di carattere: 11 pt

ha formattato: Tipo di carattere: 11 pt, Non Corsivo, Controllo ortografia e grammatica

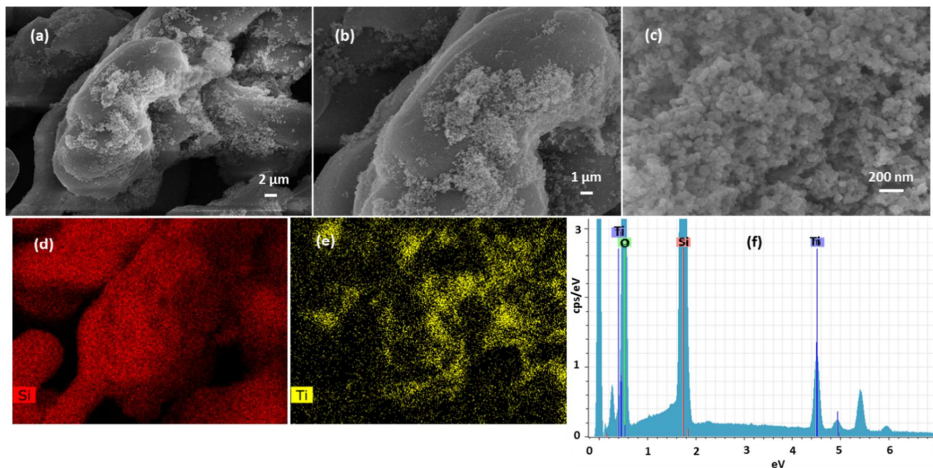


Figure 4. (a), (b), (c) SEM images of SBT10; (d) Si elemental mapping; (e) Ti elemental mapping; (f) EDX spectrum.

The optical absorption properties of TiO_2 were almost unchanged upon loading onto both SiO_2 or SBA-15 (continuous lines in Figure S5), despite the low amount of photoactive phase (10 wt. %), while the two scaffolds are completely transparent in the absorption region of TiO_2 (dashed lines in Figure S4). This suggests the transparent scaffolds to aid the TiO_2 photon absorption by improving their availability within the material thanks to the light scattering phenomenon.

The FTIR spectrum in Figure 5₂ revealed three characteristic signals for the bare TiO_2 (black line) namely the hydroxyl or adsorbed water stretching ($\nu_{\text{O-H}}$) at 3380 cm^{-1} [32] and vibration ($\delta_{\text{O-H}}$) at 1630 cm^{-1} [33], and the Ti-O bond vibration ($\nu_{\text{Ti-O}}$) at 790 cm^{-1} [34]. These features become less apparent as overlapped by the signals belonging to bare SiO_2 and SBA-15 scaffolds. On silica-based material, the most relevant signals are the adsorbed water and silanols (Si-OH) stretching vibrations at 3425 cm^{-1} ($\nu_{\text{O-H}}$) [35] and bending vibration ($\delta_{\text{O-H}}$) at 1630 cm^{-1} , plus a strong band due to Si-O-Si stretching vibrations ($\nu_{\text{O-Si-O}}$) at 1080 cm^{-1} [36]. The most relevant difference is the relative intensity of $\nu_{\text{O-H}}/\nu_{\text{O-Si-O}}$, being greater for SBA-15 and SBT10, supporting the larger and hydroxyl-rich surface of these samples compared to SiO_2 and ST10 macroporous materials.

ha formattato: Tipo di carattere: 11 pt

ha formattato: Tipo di carattere: 11 pt, Non Corsivo, Controllo ortografia e grammatica

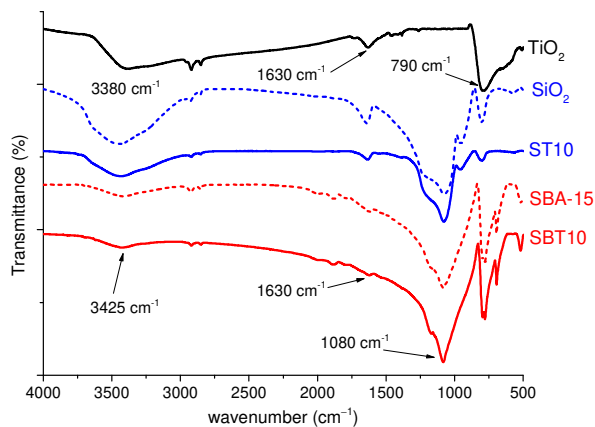


Figure 5. FTIR spectra of TiO₂, TiO₂-SiO₂ composites (continuous lines) and the bare silica scaffolds (dashed lines).

The surface composition was further analyzed by TPD. As reported in Figure S6, ST10 revealed a half peak at ca. 380-400°C, which was found regardless the sample was or not treated with a CO₂ flow (lower spectra). The following drop of the signal, observed on both ST10 and SBT10, was ascribed to the decomposition of TiO₂ which interferes with the TPD signal acquisition. The half-peak peak observed on ST10 was supposed to arise from the decomposition of surface alkaline carbonates [37] and not detected by the FTIR because probably too weak and/or overlapped with other signals. Despite further characterization would be required to better identify the nature of such species, they are supposed to be potassium-based compounds due to the presence of a potassium source (feldspar) as impurity in SiO₂.

3.3. Reactivity tests

The CO₂ photoreduction tests yielded only H₂, CH₄ and O₂ as detectable products, while CO, usually reported as a reaction product in solid-gas photocatalytic reaction [15,17], was not found in this study. The pristine and supported TiO₂ revealed some more interesting differences concerning both the activity and the selectivity. As reported in Figure 6a, the CH₄ yield was almost constant for TiO₂ and ST10 (ca. 0.7-0.8 μmol·g⁻¹·h⁻¹), while it was more than doubled on SBT10 (2.2 μmol·g⁻¹·h⁻¹). TiO₂ and SBT10 yielded H₂ as the main reduction product with a comparable selectivity, while the hydrogen evolution reaction (HER) was suppressed on ST10 (Figure 6b).

ha formattato: Tipo di carattere: 11 pt

ha formattato: Tipo di carattere: 11 pt, Non Corsivo

ha formattato: Tipo di carattere: 11 pt

ha formattato: Tipo di carattere: 11 pt, Non Corsivo, Controllo ortografia e grammatica

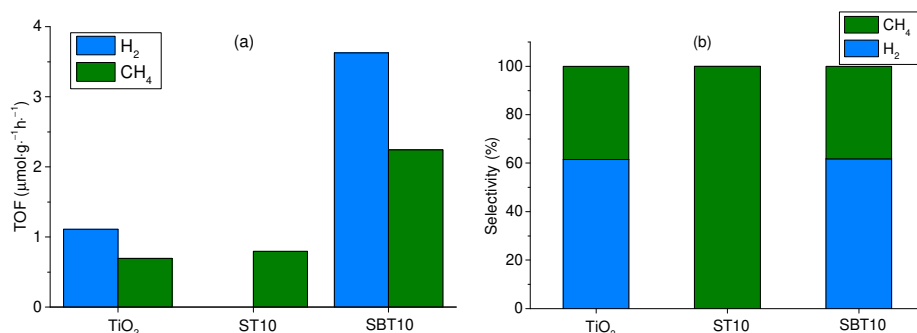


Figure 6. (a) TOF of the detected photoreduction products; (b) selectivity (%) of the photoreduction products.

The interference of organic impurities on the obtained CH₄ and H₂ is a well-known issue in CO₂ photoreduction [4,34]. To exclude their contribution, as isotope labelling of CO₂ can lead to misleading results due to the conversion of surface impurities even after cleaning pre-treatments [38], reaction tests using only H₂O as reactants (blank test) were performed. As reported in Figure S7, all the samples produced some CH₄ even in a CO₂-free reaction medium, pointing out the presence of contaminants. No H₂ was detected in these tests. However, on TiO₂ and SBT10 the activity was doubled in presence of CO₂, suggesting its actual reduction, while on ST10 surface impurities was likely to be mainly converted. To further assess the interaction with CO₂, after the 1st reaction run with H₂O, the used catalyst was exposed to a flow of CO₂ (10 mol. %) in dark conditions, and then recycled in the photoreduction with H₂O. While the pristine TiO₂ exhibited no activity, suggesting a too weak interaction with CO₂, both ST10 and SBT10 retained some activity (ca. 0.3 μmol·g⁻¹·h⁻¹) in the following two recycles (Figure 7, 2nd and 3rd). This outcomes suggests both catalysts to better interact with CO₂ rather than TiO₂, retaining this gas and then photoconverting it in presence of H₂O. Despite the lower photoactivity within a CO₂-free reaction medium, these composites are active as multifunctional materials, able to adsorb CO₂ in dark, and then to photoreduce it upon irradiation in mild conditions (T < 100°C). Furthermore, these materials were observed to have a good stability after 18 h of UVA irradiation, due to the almost constant yield of CH₄ in the 2nd and 3rd recycle tests (Figure 7). Characterizations on the spent catalysts, however, were not possible because the low amount of used catalyst (10 mg).

ha formattato: Tipo di carattere: 11 pt

ha formattato: Tipo di carattere: 11 pt, Non Corsivo, Controllo ortografia e grammatica

ha formattato: Tipo di carattere: 11 pt

ha formattato: Tipo di carattere: 11 pt, Non Corsivo

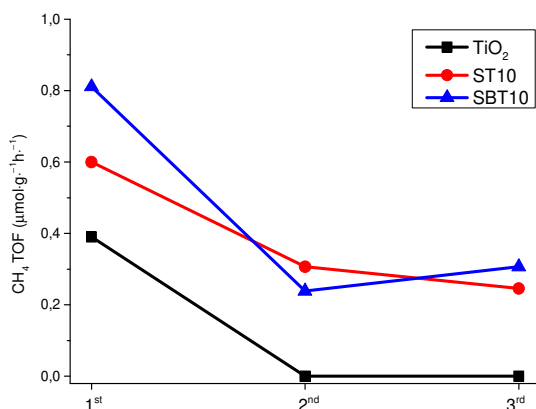


Figure 7. Reaction tests and recycles with a CO₂-free reaction medium. The used catalyst was exposed to a dark CO₂ flow prior to be re-used in the 2nd and 3rd cycles.

In the ST10 composite, the above-mentioned impurities contributing to the CH₄ production can be only partially ascribed to organic contaminants. Indeed, as suggested both by TPD analyses and the recycle tests with a dark CO₂ flow, potassium-based alkaline surface impurities was supposed to afford a good interaction of CO₂ with the scaffold by forming surface-adsorbed species such as carbonates (CO₃²⁻). Such species were then photoreduced into CH₄, regardless the presence or not of free CO₂ in the reaction medium. Furthermore, the presence of alkaline impurities that aids the CO₂ adsorption is suggested to depress the HER side reaction as well: addition of basic promoters on semiconductor photocatalysts is a well-known strategy to decrease the competition of HER [18], here played by the scaffold itself. Anyway, a more detailed identification of the nature and role of these impurities would requires further studies. Besides that, ST10 revealed a comparable activity with pure TiO₂, despite containing only 10 wt. % of active phase and having a very low SSA. The presence of the silica-based scaffold is supposed to act by “trapping” the light, by multiple reflection within the quartz microcrystals, and thus allowing more incoming photons to be absorbed by the TiO₂ on the surface (Figure 8a).

In the SBT10 composite the above-mentioned mechanism could play somehow a role, however the main reason of the enhanced catalytic activity, which exceed that of pure TiO₂ despite containing only 10 wt. % of photoactive phase, was supposed to be the large SSA. Indeed, the good adsorption properties of this mesoporous silica [17,35], are supposed to make it a huge reagent reservoir, adsorbed on its surface and then converted by the TiO₂ NPs (Figure 8b). The hydrophilicity of SBA-15 [24] and the weak interaction of CO₂ onto non-functionalized silica surface [36], are supposed to induce a competitive absorption of H₂O during the reaction, which boost up the HER in this composite. Nevertheless, despite the weak bonding with CO₂, the large SSA allows a small amount of CO₂ to be trapped within the pores upon exposing the catalyst to the dark CO₂ flow, and then photoconverted when irradiated with H₂O.

ha formattato: Tipo di carattere: 11 pt

ha formattato: Tipo di carattere: 11 pt, Non Corsivo, Controllo ortografia e grammatica

ha formattato: Tipo di carattere: 11 pt

ha formattato: Tipo di carattere: 11 pt, Non Corsivo, Controllo ortografia e grammatica

Further understanding on how to improve the activity and selectivity of these composites, could be achieved by assessing the optimum TiO₂ loading (here just 10 wt. % was used) or loading alkaline species such as alkali metal (bi)carbonates, especially on the best-performing mesoporous silica scaffolds (SBA-15). These evolutions, however, are out of the aim of this work.

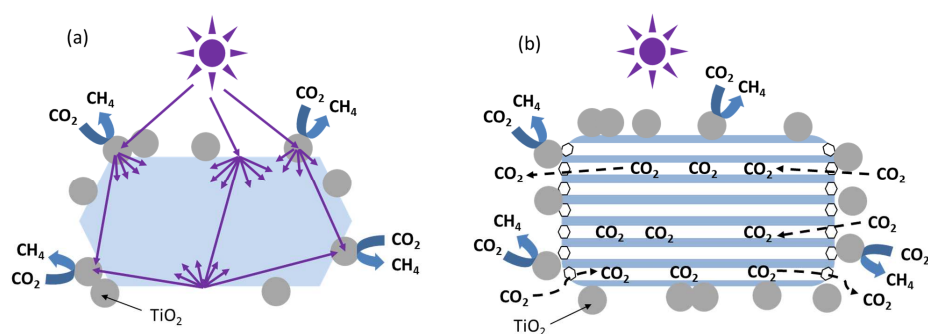


Figure 8. Proposed mechanism for photocatalytic activity enhancement of (a) ST10, where the straight arrows represent the UV rays and (b) SBT10, where the dashed arrows represent the CO₂ flow.

Conclusion

Through this work, two different silica-based materials exhibiting different morphological-structural properties were assessed as scaffolds for TiO₂ in the CO₂ photoreduction with H₂O. Exploiting a macroporous crystalline silica, the overall activity of the composite was comparable with the pure TiO₂, despite containing one tenth of the photoactive phase. Such behaviour was ascribed to the improved light harvesting thanks to the light trapping effect of the scaffold itself. Furthermore, the presence of alkaline surface impurities was supposed to improve the CO₂ adsorption and depress the competitive HER. When a high SSA mesoporous amorphous silica was involved in the composite, still using 10 wt. % of photoactive phase, the overall activity was doubled likely due to the improved reagent adsorption. Nevertheless, H₂ was detected probably due to a competitive H₂O adsorption on the hydrophilic silica surface. Finally, both the composites were also observed to retain some CO₂ from a diluted flow in dark, and then photoconvert it upon irradiation in a CO₂-free reaction medium. Despite a lower activity if compared to the CO₂-rich reaction system, this behaviour makes the composites active as multifunctional CO₂ capture/photoconverting materials, allowing the exploitation of diluted CO₂ streams. The capture ability was ascribed to different mechanism, namely to alkaline surface impurities on the macroporous scaffold, and the large SSA in the case of the mesoporous one.

Acknowledgments

The MIUR (Italian ministry for education, university and research) is gratefully acknowledged for the financial support (doctoral scholarships) of the inter-university Ph.D. program of University of Trieste and University Ca' Foscari Venice.

References

- ¹ E.V. Kondratenko, G. Mul, Jonas Baltusaitis, G.O. Larrazábal, J. Pérez-Ramírez, Status and perspectives of CO₂ conversion into fuels and chemicals by catalytic, photocatalytic and electrocatalytic processes, *Energy Environ. Sci.* 6 (2013) 3112–3135. <https://doi.org/10.1039/c3ee41272e>
- ² P. Usubharatana, D. McMartin, A. Veawab, P. Tontiwachwuthikul, Photocatalytic Process for CO₂ Emission Reduction from Industrial Flue Gas Streams, *Ind. Eng. Chem. Res.* 45 (2006) 2558–2568. <https://doi.org/10.1021/ie0505763>
- ³ A. Razzaq, S. Il In, TiO₂ based nanostructures for photocatalytic CO₂ conversion to valuable chemicals, *Micromachines.* 9 (2019) 727. <https://doi.org/10.3390/mi10050326>
- ⁴ S. Ali, M.C. Flores, A. Razzaq, S. Sorcar, C.B. Hiragond, H.R. Kim, Y.H. Park, Y. Hwang, H.S. Kim, H. Kim, E.H. Gong, J. Lee, D. Kim, S. Il In, Gas phase photocatalytic CO₂ reduction, “a brief overview for benchmarking,” *Catalysts.* 9 (2019) 1–26. <https://doi.org/10.3390/catal9090727>
- ⁵ J. Li, N. Wu, Semiconductor-based photocatalysts and photoelectrochemical cells for solar fuel generation: a review, *Catal. Sci. Technol.* 5 (2015) 1360–1384. <https://doi.org/10.1039/C4CY00974F>
- ⁶ Y. Ma, X. Wang, Y. Jia, X. Chen, H. Han, C. Li, Titanium Dioxide-Based Nanomaterials for Photocatalytic Fuel Generations, *Chem. Rev.* 114 (2014) 9987–10043. <https://doi.org/10.1021/cr500008u>
- ⁷ M.E. Aguirre, R. Zhou, A.J. Eugene, M.I. Guzman, M.A. Grela, Cu₂O/TiO₂ heterostructures for CO₂ reduction through a direct Z-scheme: Protecting Cu₂O from photocorrosion, *Appl. Catal. B Environ.* 217 (2017) 485–493. <https://doi.org/10.1016/j.apcatb.2017.05.058>
- ⁸ H. Abdullah, M.R. Khan, M. Pudukudy, Z. Yaakob, N.A. Ismail, CeO₂-TiO₂ as a visible light active catalyst for the photoreduction of CO₂ to methanol, *J. Rare Earths.* 33 (2015) 1155–1161. [https://doi.org/10.1016/S1002-0721\(14\)60540-8](https://doi.org/10.1016/S1002-0721(14)60540-8)
- ⁹ Z. Xiong, Z. Lei, C.C. Kuang, X. Chen, B. Gong, Y. Zhao, J. Zhang, C. Zheng, J.C.S. Wu, Selective photocatalytic reduction of CO₂ into CH₄ over Pt-Cu₂O TiO₂ nanocrystals: The interaction between Pt and Cu₂O cocatalysts, *Appl. Catal. B Environ.* 202 (2017) 695–703. <https://doi.org/10.1016/j.apcatb.2016.10.001>
- ¹⁰ A. Olivo, E. Ghedini, P. Pascalicchio, M. Manzoli, G. Cruciani, M. Signoretto, 2018. Sustainable Carbon Dioxide Photoreduction by a Cooperative Effect of Reactor Design and Titania Metal Promotion. *Catalysts.* 8, 41. <https://doi.org/10.3390/catal8010041>
- ¹¹ R. Chen, X. Cheng, X. Zhu, Q. Liao, L. An, D. Ye, X. He, High-performance optofluidic membrane microreactor with a mesoporous CdS/TiO₂/SBA-15@carbon paper composite membrane for the CO₂ photoreduction, *Chem. Eng. J.* 316 (2017) 911–918. <https://doi.org/10.1016/j.cej.2017.02.044>
- ¹² K. Ikeue, H. Yamashita, M. Anpo, T. Takewaki, Photocatalytic reduction of CO₂ with H₂O on Ti-β zeolite photocatalysts: Effect of the hydrophobic and hydrophilic properties, *J. Phys. Chem. B.* 105 (2001) 8350–8355. <https://doi.org/10.1021/jp010885g>
- ¹³ M. Anpo, H. Yamashita, K. Ikeue, Y. Fujii, S.G. Zhang, Y. Ichihashi, D.R. Park, Y. Suzuki, K. Koyano, T. Tatsumi, Photocatalytic reduction of CO₂ with H₂O on Ti-MCM-41 and Ti-MCM-48 mesoporous zeolite catalysts, *Catal. Today.* 44 (1998) 327–332. [https://doi.org/10.1016/S0920-5861\(98\)00206-5](https://doi.org/10.1016/S0920-5861(98)00206-5)
- ¹⁴ H.-C. Yang, H.-Y. Lin, Y.-S. Chien, J.C.-S. Wu, H.-H. Wu, Mesoporous TiO₂/SBA-15, and Cu/TiO₂/SBA-15 Composite Photocatalysts for Photoreduction of CO₂ to Methanol, *Catal. Lett.* 131 (2009) 381–387. <https://doi.org/10.1007/s10562-009-0076-y>
- ¹⁵ M. Tasbihi, F. Fresno, U. Simon, I.J. Villar-García, V. Pérez-Dieste, C. Escudero, V.A. de la Peña O’Shea, On the selectivity of CO₂ photoreduction towards CH₄ using Pt/TiO₂ catalysts supported on mesoporous silica, *Appl. Catal. B Environ.* 239 (2018) 68–76. <https://doi.org/10.1016/j.apcatb.2018.08.003>
- ¹⁶ Y. Wang, T. Li, Y. Yao, X. Li, X. Bai, C. Yin, N. Williams, S. Kang, L. Cui, L. Hu, Dramatic Enhancement of CO₂ Photoreduction by Biodegradable Light-Management Paper, *Adv. Energy Mater.* 8 (2018) 2–7. <https://doi.org/10.1002/aenm.201703136>
- ¹⁷ C. Zhao, L. Liu, Q. Zhang, J. Wang, Y. Li Photocatalytic conversion of CO₂ and H₂O to fuels by nanostructured Ce–TiO₂/SBA-15 composites, *Catal. Sci. Technol.* 2 (2012) 2558–2568. <https://doi.org/10.1039/c2cy20346d>
- ¹⁸ S. Xie, Y. Wang, Q. Zhang, W. Deng, Y. Wang, MgO- and Pt-Promoted TiO₂ as an Efficient Photocatalyst for the Preferential Reduction of Carbon Dioxide in the Presence of Water, *ACS Catal.* 4 (2014) 3644–3653. <https://doi.org/10.1021/cs500648p>
- ¹⁹ L.L. Tan, W.J. Ong, S.P. Chai, A.R. Mohamed, Photocatalytic reduction of CO₂ with H₂O over graphene oxide-supported oxygen-rich TiO₂ hybrid photocatalyst under visible light irradiation: Process and kinetic studies, *Chem. Eng. J.* 308 (2017) 248–255. <https://doi.org/10.1016/j.cej.2016.09.050>
- ²⁰ A. Steingrube, P. Voll, Selecting CO₂ Sources for CO₂ Utilization by Environmental-Merit- Order Curves, *Environ. Sci. Technol.* 50(3) (2016) 1093–1101. <https://doi.org/10.1021/acs.est.5b03474>
- ²¹ D.Y.C. Leung, G. Caramanna, M.M. Maroto-valer, An overview of current status of carbon dioxide capture and storage technologies. *Renew. Sustain. Energy Rev.* 39 (2014) 426–443. <https://doi.org/10.1016/j.rser.2014.07.093>

- ²² L. Liu, C. Zhao, J. Xu, Y. Li, Integrated CO₂ capture and photocatalytic conversion by a hybrid adsorbent/photocatalyst material. *Appl. Catal. B* 179 (2015) 489–499. <https://doi.org/10.1016/j.apcatb.2015.06.006>.
- ²³ E. Ghedini, M. Signoretto, F. Pinna, G. Cruciani, Mesoporous silica-zirconia systems for catalytic applications, *Catal. Letters*. 125 (2008) 359–370. <https://doi.org/10.1007/s10562-008-9459-8>
- ²⁴ E. Ghedini, F. Menegazzo, M. Manzoli, A. Di Michele, D. Puglia, M. Signoretto. Multifunctional and environmentally friendly TiO₂-SiO₂ mesoporous materials for sustainable green buildings. *Molecules*. 24 (2019) 4226. <https://doi.org/10.3390/molecules24234226>.
- ²⁵ S. Brunauer, P.H. Emmett, E. Teller. Adsorption of gases in multimolecular layers. *J. Am. Chem. Soc.* 60 (1938) 309–313. <https://doi.org/10.1021/ja01269a023>.
- ²⁶ P. Kubelka, F. Munk, Ein Beitrag Zur Optik Der Farbanstriche. *Z. Tech. Phys.* 12 (1931) 593–601
- ²⁷ J. Tauc, A. Mentis, States in the gap. *J. Non-Cryst. Solids* 8 (1972), 569–585, [https://doi.org/10.1016/0022-3093\(72\)90194-9](https://doi.org/10.1016/0022-3093(72)90194-9)
- ²⁸ W.T. Chen, V. Jovic, D. Sun-Waterhouse, H. Idriss, G.I.N. Waterhouse, The role of CuO in promoting photocatalytic hydrogen production over TiO₂, *Int. J. Hydrogen Energy*. 38 (2013) 15036–15048. <https://doi.org/10.1016/j.ijhydene.2013.09.101>.
- ²⁹ A. Caravaca, W. Jones, C. Hardacre, M. Bowker, 2016. H₂ production by the photocatalytic reforming of cellulose and raw biomass using Ni, Pd, Pt and Au on titania. *Proc. R. Soc. A*. 472, 20160054. <http://dx.doi.org/10.1098/rspa.2016.0054>.
- ³⁰ G. Wang, L. Xu, J. Zhang, T. Yin, D. Han, Enhanced photocatalytic activity of TiO₂ powders (P25) via calcination treatment, *Int. J. Photoenergy*. 2012 (2012) 265760. <https://doi.org/10.1155/2012/265760>.
- ³¹ J. Yu, H. Yu, B. Cheng, M. Zhou, X. Zhao, Enhanced photocatalytic activity of TiO₂ powder (P25) by hydrothermal treatment, *J. Mol. Catal. A Chem.* 253 (2006) 112–118. <https://doi.org/10.1016/j.molcata.2006.03.021>.
- ³² G. Martra, Lewis acid and base sites at the surface of microcrystalline TiO₂ anatase: relationships between surface morphology and chemical behaviour. *Appl. Catal. A*. 200 (2000) 275–285. [https://doi.org/10.1016/S0926-860X\(00\)00641-4](https://doi.org/10.1016/S0926-860X(00)00641-4).
- ³³ H. Jensen, A. Soloviev, Z. Li, E.G. Sjøgaard, XPS and FTIR investigation of the surface properties of different prepared titania nano-powders. *Appl. Surf. Sci.* 246 (2005) 239–249. <https://doi.org/10.1016/j.apsusc.2004.11.015>.
- ³⁴ T. Mahalingam, C. Selvakumar, E. Ranjith Kumar, T. Venkatachalam, Structural, optical, morphological and thermal properties of TiO₂-Al and TiO₂-Al₂O₃ composite powders by ball milling. *Phys. Lett. Sect. A* 381 (2017) 1815–1819. <https://doi.org/10.1016/j.physleta.2017.02.053>.
- ³⁵ X.S. Zhao, G.Q. Lu, A.K. Whittaker, G.J. Millar, H.Y. Zhu, Comprehensive study of surface chemistry of MCM-41 using ²⁹Si CP/MAS NMR, FTIR, pyridine-TPD, and TGA, *J. Phys. Chem. B*. 101 (1997) 6525–6531. <https://doi.org/10.1021/jp971366+>.
- ³⁶ N. Primeau, C. Vautey, M. Langlet, The effect of thermal annealing on aerosol-gel deposited SiO₂ films: A FTIR deconvolution study, *Thin Solid Films*. 310 (1997) 47–56. [https://doi.org/10.1016/S0040-6090\(97\)00340-4](https://doi.org/10.1016/S0040-6090(97)00340-4).
- ³⁷ M.S. Cho, S.C. Lee, H.J. Chae, Y.M. Kwon, H.J. Kim, M.Y. Ryu, J.B. Lee, J.C. Kim, Optimum design and characteristics of potassium-based sorbents using SiO₂ for post-combustion CO₂ capture, *Renew. Energy*. 144 (2019) 107–115. <https://doi.org/10.1016/j.renene.2018.10.057>.
- ³⁸ I. Grigioni, M.V. Dozzi, M. Bernareggi, G.L. Chiarello, E. Selli, Photocatalytic CO₂ reduction vs. H₂ production: The effects of surface carbon-containing impurities on the performance of TiO₂-based photocatalysts, *Catal. Today*. 281 (2017) 214–220. <https://doi.org/10.1016/j.cattod.2016.05.040>.
- ³⁵ B.L. Newalkar, N. V. Choudary, P. Kumar, S. Komarneni, T.S.G. Bhat, Exploring the potential of mesoporous silica, SBA-15, as an adsorbent for light hydrocarbon separation, *Chem. Mater.* 14 (2002) 304–309. <https://doi.org/10.1021/cm0106466>.
- ³⁶ X. Wang, X. Ma, C. Song, D.R. Locke, S. Siefert, R.E. Winans, J. Möllmer, M. Lange, A. Möller, R. Gläser, Molecular basket sorbents polyethylenimine-SBA-15 for CO₂ capture from flue gas: Characterization and sorption properties, *Microporous Mesoporous Mater.* 169 (2013) 103–111. <https://doi.org/10.1016/j.micromeso.2012.09.023>.
- ³⁸ T. Yui, A. Kan, C. Saitoh, K. Koike, T. Ibusuki, O. Ishitani, Photochemical reduction of CO₂ using TiO₂: Effects of organic adsorbates on TiO₂ and deposition of Pd onto TiO₂, *ACS Appl. Mater. Interfaces*. 3 (2011) 2594–2600. <https://doi.org/10.1021/am200425y>.